A phenomenological model of myelinated nerve with a dynamic threshold

R.P. Morse*, D. Allingham[1], N. G. Stocks

School of Engineering, University of Warwick, Coventry, CV4 7AL, UK

[1] Present address:

D. Allingham
School of Mathematical and Physical Sciences
University of Newcastle
Callaghan, NSW, 2308
Australia

E-mail Addresses:

R.Morse@warwick.ac.uk (R.P. Morse)
David.Allingham@newcastle.edu.au (D. Allingham)
N.G.Stocks@warwick.ac.uk (N.G. Stocks)

**Corresponding author:*

Tel: +44(0)24 765 22857
Fax +44(0)24 76 418922

Abstract

To evaluate coding strategies for cochlear implants a model of the human cochlear nerve is required. Nerve models based on voltage-clamp experiments, such as the Frankenhaeuser-Huxley model of myelinated nerve, can have over forty parameters and are not amenable for fitting to physiological data from a different animal or type of nerve. Phenomenological nerve models, such as leaky integrate-and-fire (LIF) models, have fewer parameters but have not been validated with a wide range of stimuli. In the absence of substantial cochlear nerve data, we have used data from a toad sciatic nerve for validation (50 Hz to 2 kHz with levels up to 20 dB above threshold). We show that the standard LIF model with fixed refractory properties and a single set of parameters cannot adequately predict the toad rate-level functions. Given the deficiency of this standard model, we have abstracted the dynamics of the sodium inactivation variable in the Frankenhaeuser-Huxley model to develop a phenomenological LIF model with a dynamic threshold. This nine-parameter model predicts the physiological rate-level functions much more accurately than the standard LIF model. Because of the low number of parameters, we expect to be able to optimize the model parameters so that the model is more appropriate for cochlear implant simulations.

Keywords: Leaky-integrate and fire, Frankenhaeuser-Huxley, nerve model, refractory period, cochlear implant.

1. Introduction

Although cochlear implantation has become a standard option for many children born deaf and for those who have become deaf later in life, there is still much uncertainty about how sound should be coded by a cochlear implant. To enable the evaluation of coding strategies a

computational model of the human cochlear nerve is required. Initially this could be a generic model, but the physiological properties of the cochlear nerve are known to depend on the condition of the cochlea (Shepherd and Javel, 1997) and will therefore depend on the etiology and duration of deafness. A useful model for the evaluation of coding strategies should therefore contain few parameters to enable rapid and robust fitting to patient data.

Several models of nerve fibres have been developed based on voltage-clamp experiments on nerves from a particular animal species, e.g. squid (Hodgkin and Huxley, 1952), toad (Frankenhaeuser and Huxley, 1964), rat (Schwarz and Eikhof, 1987), rabbit (Chiu et al., 1979), and human (Schwarz et al., 1995). These model the conductance or permeability of various ion channels, particularly sodium and potassium, in response to an electrical stimulus, and enable the membrane voltage to be calculated. This type of model is particularly useful for investigating the influence of specific ion channels on emergent nerve properties such as action potential duration, refractoriness, facilitation, accommodation and adaptation (e.g. Negm and Bruce, 2014; Rattay et al., 2013). Because of differences in ion channel expression, however, the systems of equations and parameters for the squid, amphibian and mammalian nerve models differ; the predicted responses to electrical stimulation therefore also differ. To date, there is no ion-channel model of the cochlear nerve based solely on cochlear-nerve recordings, although whole-cell patch clamping has enabled some ion-channels in the cochlear nerve to be identified and characterized (e.g. Santos-Sacchi, 1993; Mo and Davis, 1997; Hossain et al 2005). Moreover, there are many morphological differences between the human cochlear nerve and the cochlear nerves used in animal studies (Ota and Kimura, 1980), and these would be expected to lead substantial physiological differences (Rattay et al., 2001; Rattay et al. 2013). Nonetheless, classical ion-channel models and modified ion-channel models that incorporate classical ion-channel model have

enabled a greater understanding of how the human cochlear nerve might respond to cochlear implant stimulation (e.g. Motz and Rattay, 1986; Westen et al., 2011; Imennov et al., 2013). Ion-channel models, however, are not intended to be predictive models in the sense that they are not intended to predict the response of a particular fibre, or group of fibres. Fibres from the sciatic nerve of the toad, for example, exhibit a wide range of responses to a single stimulus (Morse and Evans, 2003) and this cannot be captured by the Frankenhaeuser-Huxley model with the single set of standard parameters. Moreover, with over forty parameters, an enormous amount of data would be required to adequately constrain the optimization of new parameter values. While ion-channel models remain useful, there is also a need for less complex models for predictive modelling.

We therefore considered using a phenomenological nerve model in which the relationships between the variables relate to observed phenomena from physiological experiments, such as the recovery from a suprathreshold pulse and the relationship between the width of a pulsatile stimulus and its threshold. Because phenomenological models generally have few parameters the parameters can be constrained by a moderate amount of data. A further advantage is that because they contain fewer equations, the computation time for phenomenological nerve models is substantially less than that for ion-channel models.

The most common phenomenological nerve model is the leaky integrate-and-fire (LIF) model, which models the membrane properties by a differential equation with a single time-constant (Lapicque, 1907). An improvement is to model the absolute refractory period following an action potential and the subsequent relative refractory period during which the threshold is elevated but gradually returns to its resting value (e.g., White, 1985); classically, the absolute refractory period is taken to be the period during which a second action potential cannot be evoked irrespective of stimulus amplitude (effectively infinite threshold), but we

discuss later that this definition may need to be refined. The recovery functions are typically exponential, but different forms, such as hyperbolic, have been used (Holden, 1976). Although the basic LIF model does not account for the probabilistic nature of the neural response this can be modelled by the addition of Gaussian noise to the threshold (Verveen and Derksen, 1968).

A few cochlear implant studies have used phenomenological models (e.g., Bruce et al., 1999a; Bruce et al., 1999b; Morse and Meyer, 2000; White, 1985; Wilson et al., 1994) and have attempted to model the phenomena described above to varying degrees. None of these models, however, have been extensively tested against cochlear nerve data. In part, this is because the technical difficulty of microelectrode recording *in vivo* has precluded the recording of responses from a single fibre to a wide variety of frequencies and amplitudes; the difficulty arises because the cochlea contains conductive fluids and the direct current between the stimulating electrodes and the recording electrode leads to a stimulus artefact that masks the neural response. If such recordings were available, it would enable much more rigorous evaluation of the cochlear nerve models.

To date, the most rigorous evaluation has been performed on the model by Bruce, et al. (Bruce et al., 1999a; Bruce et al., 1999b). The Bruce model is a stochastic model in which the input stimulus is compared with a stochastic threshold. Each spike is followed by an absolute refractory period and subsequent fixed (stimulus-independent) relative refractory period during which the threshold returns exponentially to its resting value. The model was used to predict the response to a train of biphasic pulses (100 μs per phase) presented at rates from 100 to 800 pulses per second. The Bruce model is able to accurately predict the response of single cochlear nerve fibres to these stimuli, which demonstrates the importance

of including both a stochastic threshold and refractory effects in models of the cochlear nerve.

The Bruce model, however, does not model leaky charge-integration by the nerve membrane and therefore does not include a membrane time constant. The stimuli used for validation were slowly varying compared with the time scales of the nerve being modelled, and so the inclusion of a membrane time-constant would not have greatly affected the predicted response to these particular stimuli. Without leaky charge-integration, the model would not be expected to predict the increased threshold to high-frequency sinusoids, or the effect of pulse width on the threshold to pulsatile stimulation, that have been observed in cochlear nerve experiments (Dynes and Delgutte, 1992; Kiang and Moxon, 1972). We have therefore extended the Bruce model and use a leaky integrate-and-fire neuron with a stochastic threshold. The initial model was similar to the unvalidated models by Wilson, et al. (Wilson et al., 1994), and Morse and Meyer (Morse and Meyer, 2000).

Although extensive cochlear nerve data from a single fibre is not available, we have previously recorded single-fibre data from the sciatic nerve of the toad *Xenopus laevis* in response to a wide range of stimulus frequencies and levels (Morse and Evans, 2003): frequencies were from 50 Hz to 2 kHz at levels from threshold to 20 dB above threshold. Given this data, we are adopting a three-stage approach. First, we assume that the cochlear nerve and sciatic nerve are ordinary nerves and that they share similar dynamics. This assumption is supported by our previous study, in which we measured the properties of the sciatic nerve such its excitation (strength-duration) time constant, refractory time constants, and relative spread – a measure of the internal noise level (Morse and Evans, 2003). The differences between the sciatic nerve and cochlear nerve appear to be in terms of the speed of the response and not in the intrinsic nature of the response. Based on the assumption of

shared dynamics, we here develop a phenomenological model that predicts the response of the sciatic nerve to sinusoidal stimulation. Our focus is on the application of the model to predict responses to cochlear implant stimulation and the second stage of our approach will therefore be to show that the same model (i.e. the same dynamics), but with different parameters, can adequately model the more limited cochlear nerve data. The model developed here, however, is not restricted to cochlear implants and may find application for more general studies where the predicted firing rate of a nerve fibre is required, particularly in response to high-frequency stimuli. The final stage will be to optimize the model parameters based on the compound response of the cochlear nerve to electrical stimulation by a cochlear implant (Abbas et al., 1999; Brown et al., 1996).

We first show that the standard leaky-integrate and fire model with a fixed (stimulus-independent) recovery from threshold cannot adequately predict the sciatic nerve data.

2. Leaky-integrate and fire model with fixed threshold recovery

2.1. Initial model

Our initial model was a stochastic leaky integrate-and-fire model with stimulus-independent refractory properties. The membrane time-constant, which characterizes how quickly the nerve responds to stimulation, appears in a stochastic differential equation that is solved numerically to give the membrane potential, *V(t)*, such that:

$$\tau \dot{V}(t) = -V(t) + s(t) + \sqrt{2D}\xi(t), \qquad (1)$$

where τ is the membrane time-constant, *s(t)* is the input stimulus, *D* is the noise intensity and ξ is a Gaussian white noise source, with $\langle \xi(t)\xi(t') \rangle = \delta(t-t')$ and $\langle \xi(t) \rangle = 0$; $\delta(\ldots)$ is the

Dirac delta function. Here, the stochastic term is applied to the membrane potential, rather than the threshold as in the Bruce model, but the result is the same. The stochastic term, however, in the Bruce model approximates a *1/f* noise spectrum; although this more closely matches the noise spectrum in real nerves (Verveen and Derksen, 1968), the colour of the noise would not be expected to substantially affect the results. We have used white noise to reduce the number of parameters.

Equation (1) was integrated using the two-step Heun algorithm (Kloeden et al., 1994) with a fixed step time of 5 μs. At each time-step the value of *V(t)* was compared with a fixed threshold, θ. When *V(t)* exceeded θ, an action potential ("spike") was deemed to have been evoked at time *t* and *V(t)* was reset to 0. The spike was followed by a fixed (classical) absolute refractory period (ARP), during which no integration was performed, thus holding *V(t)* at 0. This was followed by a fixed relative-refractory period, during which the recovering threshold was defined by a two time-constant exponential recovery function (Morse and Evans, 2003):

$$\theta(t) = \frac{\theta_{\text{rest}}}{1 - k\exp(\frac{\tau_{\text{abs}} - t}{\tau_1}) - (1-k)\exp(\frac{\tau_{\text{abs}} - t}{\tau_2})}, \qquad (2)$$

where *t* is the time since the conditioning pulse was applied, $k \in [0, 1]$ is the relative weighting between the two time-constants, τ_{abs} is the duration of the absolute refractory period, and τ_1 and τ_2, represent the slow long-term and fast initial threshold recovery, respectively. This function with two time-constants was found to be a better model of threshold recovery in the sciatic nerve than a single time-constant exponential form, equivalent to *k = 1* in Equation 2 (Morse and Evans, 2003).

2.2. Physiological data from the toad Xenopus laevis

The validation data for this model, and the models below, were recorded from the sciatic nerve of the toad *Xenopus laevis*. The experiments are described in detail in (Morse and Evans, 2003), but, briefly, consisted of presenting sinusoidal stimuli to a dissected nerve bundle containing several hundred nerve fibres. A microelectrode was used to measure the electrical response of individual nerve fibres and the signal was analysed to extract the times at which nerve spikes occurred. Reliable recordings could be made from a nerve for up to five hours and typically fibres were held for ten to twenty minutes; some fibres were held for over an hour. The stimuli were presented at amplitudes from just below threshold to between 5 and 20 dB above threshold. This range was chosen to ensure that responses to highly suprathreshold stimuli were recorded. The range varied between fibres because it was dependent on the stimulus threshold and was limited by the compliance of the current source used for stimulation.

Sinusoidal stimuli were presented to the fibres at frequencies of 50 Hz, 100 Hz, 200 Hz, 500 Hz, 1 kHz and 2 kHz. For frequencies less than or equal to 500 Hz, the synthesised stimuli were generated with a sampling period of 50 μs and the microelectrode recordings were sampled at 100 μs; for frequencies greater than 500 Hz, the sampling period of both the stimulus and the microelectrode recording was 20 μs. The presentation of different frequencies to a fibre was done in a random order, but all trials with a particular frequency were performed consecutively. For each frequency, five 300-ms presentations at each level were repeated such that the stimulus levels were completely randomized. For some fibres, the microelectrode recording was lost before all frequencies were presented to the fibre. We have accepted missing frequencies. We have, however, excluded data for a frequency if it was not possible to record the full set of repeats and levels. For the initial study to investigate

the fit of a standard LIF model with stimulus-independent refractoriness, only recordings from one sciatic nerve fibre (X79LF6) were used. For this fibre, we have data in steps of 2 dB. In later parts of the investigation, where we demonstrate the adequacy of the final model, we validated the model with recordings from 6 of the 36 fibres from which sinewave measurements were made; this subset included all fibres for which at least three frequencies had been presented. For all data apart from the first fibre, data were recorded in steps of 1 dB.

At each combination of frequency and level, we calculated the discharge rate (spike rate) of the responses. The first 50 ms of each response, however, was taken to be transient and was excluded from the analyses.

2.3. Parameter optimization

The six parameters of the initial model (τ, τ_{abs}, τ_1, τ_2, k, and D) were fitted to the sciatic nerve data for fibre X79LF6 using simulated annealing (Kirkpatrick et al., 1983); all results are presented relative to the resting threshold and so, without loss of generality, we fixed θ_{rest} to be 1. For the initial optimization, we optimized the model parameters separately for each frequency used in the sciatic nerve experiments, i.e. we first optimized the parameters to the sciatic nerve data for 50-Hz stimulation and then repeated the optimization for 100-Hz stimulation and so on. For a particular frequency, the objective function ("goodness") for a set of parameters was based on the similarity of the model rate-level function to that the corresponding rate-level function for the sciatic nerve. For a given set of model parameters, the model rate-level functions for sinusoidal stimulation were generated for levels from -4 dB below threshold to 30 dB above threshold in steps of 2 dB (to match the physiological data). In common with the physiological data, the discharge rate at each combination of frequency

and level was calculated for the response to 5 presentations of a 300-ms sinusoidal stimulus and the first 50 ms of each response was taken to be transient.

For a particular frequency, the goodness for each level of a rate-level function was taken to be the absolute difference between the discharge rate for the model and the corresponding discharge rate for the sciatic nerve data divided by standard deviation for the sciatic nerve data for the five presentations, i.e. it was a *z*-score. The goodness for a particular frequency was the sum of the *z*-scores for the levels where there was both sciatic nerve and model data. To compensate for possible errors in the measured thresholds for the sciatic nerve, we calculated the goodness for the model rate-level functions with shifts of up to ±2 dB in the corresponding sciatic nerve rate-level function; we took the overall goodness for a particular frequency to be the minimum of these.

2.4. Results

Fig. 1 shows the optimal fits of the model rate-level functions to the rate level functions for a single sciatic nerve fibre. With the parameters optimized separately at each frequency the fits are excellent. Except at 50 Hz, the model correctly predicted the maximum discharge rate for the nerve fibre and the model rate-level functions had the same plateaus and transitions as the level was increased. Even at 50 Hz the correspondence between the model and the sciatic nerve data was very close, although for the best parameters found the model did not predict the decrease in discharge rate at the highest level.

On this basis it might be thought that the standard leaky integrate-and-fire model with a fixed recovery from threshold is a good model of the sciatic nerve. An inspection, however, of the optimal model parameters at each frequency showed that the optimal value of the absolute refractory period changed systematically with frequency (Fig. 2). For frequencies less than

500 Hz, the optimal absolute refractory period was about 4 ms. For frequencies at 500 Hz and above the optimal absolute refractory period was less than 1 ms. When the optimal parameters for one frequency were used to generate rate-level functions at other frequencies there was a poor correspondence between the model and sciatic nerve rate-level functions at all frequencies other than the optimized frequency. An example is shown in Fig. 3, which shows the sciatic rate-level functions and those predicted by the model with parameters optimized for 50-Hz stimulation; for this frequency the optimal absolute refractory period was 4.4 ms. Even for 100-Hz stimulation there was a marked discrepancy between the predicted and actual rate-level functions, with the model having a more gradual change in discharge rate with level. At higher frequencies, the large absolute refractory period resulted in a substantial underestimation of the discharge rate; for example at 2000 Hz the maximum discharge rate from the sciatic nerve fibre was 2000 spikes / s whilst the maximum rate from the model was 220 spikes / s. Similarly, the optimal fits for high-frequency stimulation led to poor predictions of the rate-level functions for low-frequency stimulation. With the small absolute-refractory period required to predict high discharge rates at high frequencies there were multiple discharges in the model response to each period of a low-frequency stimulus; the model therefore predicted substantially too many discharges.

2.5. Discussion

These results highlight the importance of fitting nerve models to extensive physiological data. With model parameters fitted to data at a single frequency, or a narrow range of frequencies, it might incorrectly be concluded that the LIF model with a fixed recovery function is a good nerve model. The results, however, suggest that the refractory properties of a nerve fibre may be dependent on the nature of the stimulation during the refractory period.

Further evidence that refractoriness is stimulus dependent comes from our companion study using the Frankenhaeuser-Huxley model of nerve fibre. The Frankenhaeuser-Huxley (FH) model (Frankenhaeuser and Huxley, 1964) is based on physiological measurements from the sciatic nerve of *Xenopus laevis*, which corresponds to the preparation we used in our physiological study (Section 2.2). Standard models of threshold recovery following an action potential have been based on physiological experiments using a two-pulse paradigm in which the first "conditioning" pulse causes excitation and the second pulse is used to determine the threshold at various intervals following the first (e.g. Amberson, 1930; Erlanger et al., 1927; Forbes et al., 1923; Miller et al., 2001). In our study, we used a three-pulse paradigm in which an intermediate depolarizing pulse was presented immediately following a 10-μs suprathreshold conditioning pulse, and was therefore in the refractory period. We showed that applying a depolarizing stimulus during the later part of what is classically regarded as the absolute refractory period could effectively prolong the absolute refractory period, while leaving the refractory time-constants and other refractory parameters largely unaffected. We further showed with sinusoidal signals that stimulation during the classical absolute refractory period could suppress excitation. In particular, a segment of a sinewave that in isolation caused excitation could suppress an action potential if it fell within the absolute refractory period. We concluded that the classical definition of absolute refractory period should be refined to include only the initial period following an action potential when on-going stimulation does not affect the threshold; this period was found to be about half as long as the classical absolute refractory period.

For studies with a LIF model that involve only sinusoidal stimulation, it might be adequate to retain the standard recovery function but make the absolute refractory period frequency-dependent using a function based on the results shown in Fig. 2. With more arbitrary

stimulation, however, like those used in cochlear implants, such compensation is not possible and a different way of introducing stimulus-dependent refractoriness is required. As described in the following section, we considered that a greater understanding of threshold recovery in the FH model and how it relates to the activation and inactivation of the various ion channels might enable the LIF model to be extended so that it demonstrates stimulus-dependent refractoriness.

3. Recovery from threshold in the Frankenhaeuser-Huxley model

The Frankenhaeuser-Huxley model simulates the activation and inactivation states of the sodium channels (represented by *m* and *h*, respectively), the activation state of the potassium channel (represented by *n*) and activation state of a non-specific ion channel (represented by *p*). We considered that if threshold is closely related to any of the activation or inactivation variables then stimulus-dependent refractoriness could be introduced into the LIF model by approximating the voltage dependence of one of the gating variables. We investigated the relationship between threshold and the gating variables using the same three-pulse paradigm that we used in our companion study.

3.1. Methods

The methods for the FH simulation and a description of the three-pulse paradigm are given in Morse et al. (2015). In brief, the conditioner pulse had a duration of 10 μs and an amplitude 1 dB above the resting threshold of 60.61 A / m^2. The short pulse duration was chosen to approximate a near-instantaneous application of current and the level of the conditioner was such that it led to excitation in response to every presentation. As for the standard two-pulse paradigm used to measure the recovery function, we determined the threshold of a probe pulse that occurred at an interval after the conditioner pulse; the probe pulse also had a

duration of 10 μs. With the three-pulse paradigm, however, there was an additional depolarizing pulse immediately following the conditioner pulse. In this study, we measured the threshold of the probe pulse for conditioner-probe intervals of 2 ms, 5 ms, 10 ms and 20 ms for a simulated temperature of 20 °C; for the longest interval, we expected the threshold to have returned to its resting value in the absence of an intermediate pulse. For each conditioner-probe interval, the probe threshold was recorded for a range of durations and amplitudes of the intermediate pulse. Because the duration of the probe pulse was short compared with the time-scales of the model, we could approximate the instantaneous nerve threshold to be the threshold amplitude of the probe pulse. For the threshold level of the probe pulse we also recorded the value of the four activation and inactivation variables (*m*, *h*, *n*, and *p*) at the instant of the probe pulse. The duration of the intermediate pulse was from 500 μs to 500 μs less than the conditioner-probe interval in steps of 250 μs. The amplitude of the intermediate pulse was -30 dB, -24 dB, -12 dB or -6 dB relative to the resting threshold for a 10-μs pulse. From the previous study, the ranges in intermediate pulse amplitude and duration were known to produce a range of effect on threshold from negligible to substantial. Some combinations of intermediate pulse amplitude and duration led to additional action potentials following the conditioning pulse even in the absence of a suprathreshold probe pulse.

3.2. Results and discussion

The relationship between the threshold amplitude of a probe pulse and the gating variables of the FH model at the instant of the probe for the three pulse paradigm are shown in Fig. 4. The plots for each gating variable against threshold were greatly overlapping for the combinations of conditioner-pulse interval, intermediate pulse amplitude, and intermediate pulse duration; this overlap occurred both when the nerve was approximately it its resting

state and when the nerve was deep within the refractory period and the threshold was about four times its resting value. The functions relating each gating variable to threshold are therefore largely independent of the stimulus preceding the probe pulse over the range of intermediate pulse investigated. Given that the functions relating threshold and the gating variables were largely independent of the stimulus preceding the probe pulse then given the value of any gating variable we can calculate the instantaneous membrane potential that will result in an action potential. This threshold potential, however, is dependent on the past history of the stimulus because the gating variables are dependent on the membrane potential (Frankenhaeuser and Huxley, 1964), which is stimulus-dependent. Given these findings, we have replaced the fixed refractory properties of the initial LIF model by a dynamic threshold that approximates the dynamics of one of the gating variables.

4. Development of a LIF model with stimulus-dependent refractoriness

We chose to approximate the sodium inactivation variable, *h*, as this had the largest variation with threshold and we considered that this would lessen the sensitivity of the model.

We approximated the curve shown in Fig. 4b by the function

$$\theta(h) = \frac{\theta_M}{h^P} + \theta_o \,, \qquad (3)$$

where θ_M, θ_o, and P are constants. All results are presented relative to the resting threshold and so, without loss of generality, we have fixed θ_o at 1.

Using this function we can find the threshold at any given time, *t*, by calculating *h(t)* using the equation from the FH model. This is an ordinary differential equation with 6 rate parameters that relates *h* and the membrane potential, *V*, by

$$\tau_h \dot{h} = -h + h_\infty , \tag{4}$$

where

$$\tau_h = \frac{1}{\alpha_h + \beta_h} \tag{5}$$

and

$$h_\infty = \frac{\alpha_h}{\alpha_h + \beta_h}. \tag{6}$$

In the FH model α_h and β_h are given by

$$\alpha_h = \frac{A_\alpha (B_\alpha - V)}{1 - \exp\left(\frac{V - B_\alpha}{C_\alpha}\right)}, \tag{7}$$

and

$$\beta_h = \frac{A_\beta}{1 + \exp\left(\frac{B_\beta - V}{C_\beta}\right)}, \tag{8}$$

The relationships between the membrane voltage, *V*, and the steady-state value of the sodium inactivation variable, h_∞, and the time constant of the sodium inactivation variable, τ_h are

shown in Fig. 5 for the values of the constant A, B, and C (with the various subscripts) as given by Frankenhaeuer and Huxley. For our dynamic threshold model we approximated h_∞ in Equation 4 with the Boltzmann sigmoidal curve

$$h_\infty = \left[1 + \exp\left(\frac{V - \mu_\infty}{\sigma_\infty}\right)\right]^{-1}. \quad (9)$$

where μ_∞ is the offset of the sigmoidal curve and σ_∞ defines its width. We fixed τ_h as a constant. A Gaussian function or similar could have been used to approximate τ_h, but, as shown below, we obtained good results for sinusoidal stimulation using constant τ_h and so retained this further simplification.

Our final model is obtained by combining the standard stochastic leaky integrate-and-fire model from Equation (1) with the dynamic threshold from Equation (3), where h is given by Equation 4 and h_∞ is approximated as described above. When V exceeds the threshold, a spike is deemed to have been evoked and V and h are reset to 0 and held at that value during the absolute refractory period. Here we use the term "absolute refractory period" and the associated model parameter, τ_{ABS}, in accord with the refined terminology we give in Morse et al. (2015), i.e. it is the period immediately following an action potential during which an ongoing stimulus does not affect the threshold. Immediately after this period the threshold again becomes dynamic. The dynamic threshold is initially large following the absolute refractory period, but in the absence of further stimulation it will return to its resting value.

Our modified LIF model with dynamic threshold has nine parameters: τ, the membrane time constant; τ_{ABS}, the absolute refractory period; τ_h, the recovery time-constant for h; D, the internal noise intensity; θ_o, the base value of the threshold; θ_M, the threshold multiplier; μ_∞,

the offset for h_∞; σ_∞, the standard deviation of h_∞; and P, the power of h in the threshold equation (Equation 3).

4.1. Parameter optimization for FH model

To demonstrate that the LIF model with a dynamic threshold approximates the dynamics of the FH model we optimized the parameters of the LIF model to fit rate-level functions calculated with the FH model. The rate-functions for the FH model were generated for sinusoidal stimulation at frequencies of 50 Hz, 100 Hz, 200 Hz, 500 Hz, 1 kHz and 2 kHz with levels from -4 dB below threshold to 20 dB above threshold in steps of 1 dB. Because the FH model is deterministic we fixed the noise intensity, D, to be 0. The remaining eight parameters of the modified LIF model were fitted to the FH data using similar methods to those used to fit the initial LIF model to the sciatic nerve data. The modified LIF model parameters, however, were optimized to get the best fit over all frequencies rather than for a single frequency. For a given set of model parameters, the LIF rate-level functions were generated at the same frequencies as for the FH model but with a maximum level of 30 dB above threshold; the maximum level for the FH model (20 dB) was lower to ensure that the the regenerative component of the membrane voltage could be clearly distinguished from the capacitive component. At each frequency, the goodness for each level of a rate-level function was taken to be the least-squares difference between the rate-level functions normalized by the maximum discharge rate for the FH model at that frequency. The normalization was used so that the different frequencies contributed equally to the overall goodness (a *z*-score was not used because the FH model is deterministic and no variability is therefore expected). The goodness for a particular frequency was the sum of the goodness values over the levels where there was both sciatic nerve and model data. The overall goodness for a set of parameters was the sum of the goodness values for each frequency.

To study the dynamic threshold properties of the modified LIF, we used the optimized parameters from above in a simulation with the same three-pulse paradigm that was used for the FH model (Morse et al., 2015). A 10-μs conditioning pulse 1 dB above threshold was immediately followed by a depolarizing 1000-μs intermediate pulse: in the control condition, the intermediate pulse had zero amplitude and in the two experimental conditions the amplitude was -24 dB or -18 dB relative to the conditioner threshold. For each amplitude of the intermediate pulse, the threshold recovery function was determined by finding the minimum conditioner-probe interval that led to excitation for probe amplitudes from 0 to 10 dB above the resting threshold.

4.2. Results

The optimal fitted parameters of the LIF model with a dynamic threshold are given in Table I. A comparison of the rate-level functions for the modified LIF model with these parameters and those calculated with the FH model are shown in Fig. 6. The overall agreement between the rate-level functions is very good at each frequency tested. The modified LIF model captured the discharge rate at the maximum stimulus level, and finer detail such as the gradual change in discharge rate with stimulus level interspersed with plateaus where the discharge rate was constant over a range of levels. It is notable that the modified LIF model captured the non-monontonic change in discharge rate with level for 50-Hz stimulation, where for medium stimulus levels (7-10 dB above threshold) the FH model produced two spikes per period.

The threshold recovery functions for the modified LIF model with the same optimized parameters are shown in Fig. 7. For the threshold recovery without an intermediate pulse the least-squares best fit of the double exponential function (Equation 2) gave τ_{abs} = 1.20 ms, τ_1 =

1.43 ms, τ_2, = 2.7 μs, and k = 0.47. The addition of a depolarizing intermediate pulse, however, delayed recovery. With a 1000-μs intermediate 18 dB below the threshold of the 10-μs conditioner, recovery was delayed by about 2 ms.

4.3. Discussion

The threshold for the modified LIF model was based on the dynamics of a gating variable in the FH model with the intention of making the threshold dependent on the stimulus. The results show that this intention has been met. In contrast to a LIF model with a fixed recovery function, one set of parameters was sufficient to capture the rate-level dynamics of the FH model over a wide range of stimulus amplitudes and frequencies. Moreover, the recovery functions in Fig. 7 directly show that the threshold for the modified LIF model is stimulus dependent.

For the new model, threshold in the relative refractory period is an emergent property that is affected by a number of variables rather than just being a function of the time since the previous action potential. Nonetheless, in the absence of stimulation during the relative refractory period, the recovery function was well described by the fixed recovery model given by Equation 2 (Fig. 7). With stimulation less than 1.20 ms following the conditioner, the threshold was effectively infinite. This closely corresponds to the classically defined absolute refractory period of 1.23 ms for the FH model; we emphasize again that this period differs from the shorter absolute refractory period in the model, τ_{ABS}, as this is the time during which ongoing stimulation does not affect the threshold. The longer threshold recovery time-constant of 1.43 ms for the modified LIF model was also similar to the corresponding time-constant for the FH model, which was 1.65 ms. The shorter threshold recovery time-constants, however, were quite different between the models (27 μs for the

modified LIF model and 248 μs for the FH model). More accurate prediction of the initial threshold recovery would require a more complex model, but we nonetheless consider our extension to the LIF model to be useful. This is shown by the close approximation of the LIF model rate-level functions to those from the FH model. The usefulness of the model to predict real physiological data is demonstrated in the following section.

5. Fit of the leaky integrate-and-fire model with stimulus-dependent refractoriness to the sciatic nerve data

We fit the modified LIF model to the sciatic nerve rate-level data using similar methods to those given in Section 2 for the standard LIF model. In common with the optimization for the FH data, however, the modified LIF model parameters were optimized to get the best fit over all frequencies rather than for a single frequency. In initial fits, we allowed P to vary, but the values were typically about 1.3 (as for the FH model above) and we therefore fixed this parameter at 1.3 for the final fits.

Using the optimal parameters based on these rate-level fits, we compared the temporal responses of the modified LIF model with the sciatic nerve data. Period histograms (PHs) and inter-spike interval histograms (ISIHs) for the modified LIF model and sciatic nerve were constructed from the responses to the five presentations at each level and frequency using standard methods (Gerstein and Kiang, 1960). As for the rate-level functions, the first 50 ms of each 300-ms response was taken to be transient and discarded from the analyses. The bin width for the PHs and ISIHs was 100 μs for frequencies less than 1 kHz and 20 μs for frequencies above.

5.1. Results

The optimal parameters for each fibre are given in Table 1. Although we included the noise intensity, *D*, as a parameter it was not well-constrained by the sciatic nerve data; changes in D by a factor of 100 made negligible difference the predicted rate-level functions. We have nonetheless included the optimized values for *D* in Table I for completeness.

A comparison of the rate-level functions predicted by the modified LIF model and those observed physiologically from the sciatic nerve is shown in Fig. 8. The overall agreement between the model results and the physiological data is very good for all the fibres. With a single set of parameters for each fibre, the modified LIF model captured the change in discharge rate with stimulus level across a wide range of levels and frequencies. This is particularly notable because there was a lot of variability in the physiological data: fibre X79LF6, for example, had a discharge rate of 2000 spikes / s for a 2-kHz stimulus 20 dB above threshold whilst for fibre X82RF3 the equivalent discharge rate was less than 400 spikes / s. Likewise, at high stimulus levels fibres X79LF6 and X82RF3 could fire twice per period in response to 50-Hz stimulation whilst the other fibres produced at most one spike per period.

Although all the model parameters were fitted only to the sciatic nerve rate-level functions, the modified LIF model largely predicted the temporal characteristics of the sciatic nerve (Fig. 9). As shown for the optimized fit for fibre X80LF3, the period histograms for the modified LIF model and the sciatic nerve fibre were similar (Fig. 9a). The tighter phase-locking in response to higher stimulus levels is evident in both the model and the sciatic nerve fibre by the narrower peaks in the PHs. Furthermore, at higher stimulus levels, there was a distinct decrease in the latency between the start of the stimulus period and the time of

evoked spikes for both the model and the real fibre. The distribution, however, of spike times in the PHs for the model were narrower than those for the nerve fibre. The decrease in latency with stimulus level was also less for the model than for the real nerve.

There was also a close correspondence between the ISIHs for the model and those for the sciatic nerve fibres. At all stimulus levels and stimulus frequencies, the positions of the peaks in the ISIHs for the model and real nerve are almost identical. The amplitudes of the peaks, however, were smaller for the modified LIF model than for the fibres. This resulted from the slightly wider distribution of each peak for the modified LIF model, which was also evident in the PHs. The ISIHs for the X80LF3 show that the inter-spike intervals were at multiples of the stimulus period. This indicates that a spike was not evoked by every period of the stimulus, but when it was it tended to be phase-locked to the stimulus. The pattern of inter-spike intervals was similar for the model, but it is notable that there were fewer long inter-spike intervals for the model at low stimulus levels.

5.2. Discussion and conclusions

We have shown that the LIF model with a dynamic threshold and a single set of parameters can predict the rate-level functions of real nerve fibres over a wide range of stimulus amplitudes and frequencies. The correspondence between the physiological data and this model was much closer than could be found with a LIF model with fixed refractory properties and a fixed threshold (Section 2). We could not find parameters for the modified LIF model that predicted the non-monotonic response of fibre X79LF6 in response to high amplitude 50-Hz stimulation. The parameters that we did obtain, however, provide an excellent fit at other frequencies and stimulus levels, and parameters for fibre X82RF3 were able to predict the double firing for that fibre at 50 Hz. We note that the model was able to

predict the non-monotonic response to 50-Hz stimulation for the FH model. It may be that some set of parameters would be able to predict the non-monotonic rate-level function for X91LF6 at 50 Hz and also give a good fit at other frequencies. Our long-term aim, however, is to optimize the model for cochlear nerve data rather than for a single sciatic nerve fibre and we did not therefore exhaustively search for parameters for this fibre.

As noted earlier, it was not possible to record responses to all the stimulus frequencies from all the sciatic nerve fibres. Moreover, because of variations in thresholds and the compliance limitations for the current source, the maximum stimulus levels varied across fibres. Nonetheless, the extrapolations for the model appear to be physiologically plausible, given that for combinations of frequency and level where it was not possible to record physiological data, the pattern of predicted discharge rates were consistent with those from fibres where data were obtained. For example, the predicted rate-level functions for X79RF1 at 1000 Hz and 2000 Hz are similar to the actual rate-level functions for fibre X80LF3.

The tighter phase locking for the model may partially have resulted from the noise intensity, *D*, being too low. As stated above, the optimization to the rate-level functions did not constrain the noise intensity and it could have been substantially larger; this would have broadened the PHs without grossly affecting the rate-level functions. The level of noise could be constrained by knowledge of the "relative spread", which is a measure of internal noise level based on the change in firing efficiency with level for pulsatile stimuli (Verveen, 1960). We have measured relative spread for sciatic nerve fibres in general, but not specifically for the fibres for which we have the rate-level functions. An additional variability in the sciatic nerve response would have been expected from jitter, which is the variance in the conduction time. Such variability has been observed in the electrically stimulated cochlear nerve (Anderson, 1973; Miller et al., 1999). To model the jitter we could

introduce a random shift in spike times, but we have limited the model at this stage to being a model solely of excitation. It would be useful, however, to have a phenomenological conduction model that included jitter and also modelled the large changes in latency with level that were observed with the sciatic nerve but not predicted by the modified LIF model. This effect might be modelled by consideration of the known changes in conduction velocity during the relative refractory period (Forbes et al., 1923).

The current model fulfils our objectives for an excitation model. The model has about 25 % fewer parameters than standard ion-channel models and yet is able to predict the response to sinusoidal stimuli over a wide range of stimulus amplitudes and frequencies. Although the fits were based on physiological responses to sinusoids, the wide range of stimuli should mean the model is equally appropriate for pulsatile stimuli or more complex stimuli such as speech. Equally importantly, the low number of parameters and differential equations mean that the model is computationally fast and can be constrained by a moderate amount of physiological data. We therefore expect to be able to adapt the model parameters to those more appropriate for cochlear implant simulations.

Acknowledgements

This work was funded in part by the MRC (grant G0001114) and the EPSRC (grant GR/35650/01).

References

Abbas, P. J., Brown, C. J., Shallop, J. K., Firszt, J. B., Hughes, M. L., Hong, S. H., Staller, S. J., 1999. Summary of results using the Nucleus CI24M implant to record the electrically evoked compound action potential. Ear and Hearing 20, 45-59.

Amberson, W. R., 1930. The effect of temperature upon the absolute refractory period in nerve. Journal of Physiology 69, 60-66.

Anderson, D. J., 1973. Quantitative model for the effects of stimulus frequency on synchronization of auditory nerve discharges. Journal of the Acoustical Society of America 54, 361-364.

Brown, C. J., Abbas, P. J., Borland, J., Bertschy, M. R., 1996. Electrically evoked whole nerve action potentials in Ineraid cochlear implant users: responses to different stimulating electrode configurations and comparison to psychophysical responses. Journal of Speech and Hearing Research 39, 453-467.

Bruce, I. C., Irlicht, L. S., White, M. W., O'Leary, S. J., Dynes, S., Javel, E., Clark, G. M., 1999a. A stochastic model of the electrically stimulated auditory nerve: pulse-train response. IEEE Transactions on Biomedical Engineering 46, 630-637.

Bruce, I. C., White, M. W., Irlicht, L. S., O'Leary, S. J., Dynes, S., Javel, E., Clark, G. M., 1999b. A stochastic model of the electrically stimulated auditory nerve: Single-pulse response. IEEE Transactions on Biomedical Engineering 46, 617-629.

Chiu, S. Y., Ritchie, J. M., Rogart, R. B., Stagg, D., 1979. A quantitative description of membrane currents in rabbit myelinated nerve. Journal of Physiology 292, 149-166.

Dynes, S. B. C., Delgutte, B., 1992. Phase-locking of auditory nerve discharges to sinusoidal electric stimulation of the cochlea. Hearing Research 58, 79-90.

Erlanger, J., Gasser, H. S., Bishop, G. H., 1927. The absolute refractory phase of the alpha, beta and gamma fibers in the sciatic nerve of the frog. American Journal of Physiology 81, 473-474.

Forbes, A., Ray, L. H., Griffith, F. R., Jr., 1923. The nature of the delay in the response to the second of two stimuli in nerve and in nerve-muscle preparation. American Journal of Physiology 66, 553-617.

Frankenhaeuser, B., Huxley, A. F., 1964. The action potential of the myelinated nerve fibre of Xenopus laevis as computed on the basis of voltage clamp data. Journal of Physiology 171, 302-315.

Gerstein, G., Kiang, N. Y. S., 1960. An approach to the quantitative analysis of electrophysiological data from single neurons. Biophysical Journal 1, 15-28.

Hodgkin, A. L., Huxley, A. F., 1952. A quantitative description of membrane current and its application to conduction and excitation in nerve. Journal of Physiology 117, 500-544.

Holden, A., 1976. Models of the stochastic activity of neurons. Springer-Verlag, Berlin.

Hossain, W. A., Antic, S. D., Yang, Y., Rasband, M. N., Morest, D. K., 2005. Where is the spike generator of the cochlear nerve? Voltage-gated sodium channels in the mouse cochlea. Journal of Neuroscience, 25, 6857-6868.

Imennov, N.S., Won, J.H., Ward, D.R., Drennan, R., Jameyson, E., & Rubinstein, J.T. (2013). Detection of acoustic temporal fine structure by cochlear implant listeners: Behavioral results and computational modelling. Hearing Research, 298, 60-72.

Kiang, N. Y. S., Moxon, E. C., 1972. Physiological considerations in artificial stimulation of the inner ear. Annals of Otology Rhinology Laryngology 81, 714-730.

Kirkpatrick, S., Gelatt, C. D., Vecchi, M. P., 1983. Optimization by Simulated Annealing. Science 220, 671-680.

Kloeden, P., Platen, E., Schurz, H., 1994. Numerical Solution of SDE Through Computer Experiments. Springer-Verlag, Berlin.

Lapicque, L., 1907. Sur l'excitation électrique des neufs. Journal of Physiology (Paris) 9, 620-635.

Miller, C. A., Abbas, P. J., Robinson, B. K., 2001. Response properties of the refractory auditory nerve fiber. Journal of the Association for Research in Otolaryngology 2, 216-232.

Miller, C. A., Abbas, P., Robinson, B. K., Rubinstein, J. T., Matsuoka, A. J., 1999. Electrically evoked single-fiber action potentials from cat: responses to monopolar monophasic stimulation. Hearing Research 130, 197-218.

Mo, Z. L., Davis, R. L., 1997. Heterogeneous voltage dependence of inward rectifier currents in spiral ganglion neurons. Journal of Neurophysiology, 78, 3019-3027.

Morse, R. P., Meyer, G. F., 2000. The practical use of noise to improve speech coding by analogue cochlear implants. Chaos, Solitons and Fractals 11, 1885-1894.

Morse, R. P., Evans, E. F., 2003. The sciatic nerve of the toad *Xenopus laevis* as a physiological model of the human cochlear nerve. Hearing Research 182, 97-118.

Morse, R. P., Allingham, D., Stocks, N. G., 2015. Stimulus-dependent refractoriness in the Frankenhaeuser-Huxley model. Journal of Theoretical Biology submitted for publication.

Motz, H., Rattay, F., 1986. A study of the application of the Hodgkin-Huxley and the Frankenhaeuser-Huxley model for electrical stimulation of the acoustic nerve. Neuroscience 18, 699-712.

Ota, C.Y., Kimura, R.S., 1980. Ultrastructural study of the human spiral ganglion. Acta Otolaryngology, 89, 53-62.

Rattay, F., Aberham, M., 1993. Modelling axon membranes for functional electrical stimulation. IEEE Transactions on Biomedical Engineering 40, 1201-1209.

Rattay, F., Lutter, P., Felix, H., 2001. A model of the electrically excited human cochlear neuron I. Contribution of neural substructures to the generation and propagation of spikes. Hearing Research, 153, 43-63.

Rattay, F., Potrusil, T., Wenger, C., Wise, A.K., Glueckert, R., Schrott-Fischer, A., 2013. Impact of Morphometry, Myelinization and Synaptic Current Strength on Spike Conduction in Human and Cat Spiral Ganglion Neurons. Plos One, 8, 1-16.

Santos-Sacchi, J., 1993. Voltage-dependent ionic conductances in Type I spiral ganglion cells from the guinea pig inner ear. Journal of Neuroscience, 13, 3599-3611.

Schwarz, J. R., Eikhof, G., 1987. Na currents and action potentials in rat myelinated nerve fibres at 20 and 37 °C. Pflügers Archive 409, 569-577.

Schwarz, J. R., Reid, G., Bostock, H., 1995. Action potentials and membrane currents in human node of Ranvier. Pflügers Archive 430, 283-292.

Shepherd, R. K., Javel, E., 1997. Electrical stimulation of the auditory nerve. I. Correlation of physiological response with cochlear status. Hearing Research 108, 112-144.

Verveen, A. A., 1960. On the fluctuation of the threshold of the nerve fiber. In: Tower, D. B., Schadé, J. P., Eds.), Structure and function of the cerebral cortex. Elsevier, Amsterdam, pp. 282-288.

Verveen, A. A., Derksen, H. E., 1968. Fluctuation phenomena in nerve membrane. Proceedings of the IEEE 56, 906-916.

Westen, A. A., Dekker, D. M. T., Briaire, J. J., Frijns, J. H. M., 2011. Stimulus level effects on neural excitation and eCAP amplitude. Hearing Research, 280, 166-176.

White, M. W., 1985. Speech and stimulus coding strategies for cochlear implants. In: Schindler, R. A., Merzenich, M. M., Eds.), Cochlear implants. Raven Press, New York, pp. 243-267.

Wilson, B., Finley, C., Zerbi, M., Lawson, D. T., 1994. Speech processors for auditory prostheses: 7th Quarterly NIH Report N01-DC-2-2401. Research Triangle Institute.

Table legends

Table I. Fitted parameters for the leaky integrate-and-fire model with a dynamic threshold. The parameters are: τ, the membrane time constant; τ_{abs}, the absolute refractory period; τ_h, the recovery time-constant for h; D, the internal noise intensity; θ_o, the base value of the threshold; θ_M, the threshold multiplier; μ_∞, the offset for h_∞; σ_∞, the standard deviation of h_∞; and P, the power of h in the threshold equation (Equation 3). Parameters are given for fits to the Frankenhaeuser-Huxley model and six sciatic nerve fibres.

Figure legends

Fig. 1. Optimum rate-level functions (plots of discharge rate against stimulus level) for a leaky integrate-and-fire model with a stimulus-independent recovery function in response to sinusoidal stimulation from 50 Hz to 2 kHz. The model parameters were optimized separately for each frequency (solid lines) to get the best fit to rate-level functions from sciatic nerve fibre X79LF6; the means for the sciatic nerve (5 presentations) are shown by the solid dots and the error bars show the standard deviation. The stimulus levels are in dB relative to the threshold for the particular frequency.

Fig. 2. Optimum values of the absolute refractory period for a stimulus-independent recovery function (Equation 2) in response to sinusoidal stimulation from 50 Hz to 2 kHz.

Fig. 3. Rate-level functions (solid lines) for a leaky integrate-and-fire model with a stimulus-independent recovery function in response to sinusoidal stimulation from 50 Hz to 2 kHz. The model parameters were optimized to get the best fit to the sciatic nerve rate-level from fibre X79LF6 at 50 Hz. The means for the sciatic nerve (5 presentations) are shown by the

solid dots and the error bars show the standard deviation. The stimulus levels are in dB relative to the threshold for the particular frequency.

Fig. 4. Relationship between the relative threshold of a probe pulse and the activation and inactivation variables of the Frankenhaeuser-Huxley model at the instant of the probe for a three-pulse paradigm. The thresholds are relative to the resting threshold of the 10-μs probe. Simulations were done with conditioner-probe intervals of 2 ms, 5 ms, 10 ms, and 20 ms. For each conditioner-probe interval, overlapping curves are shown for intermediate pulse durations of 500 μs up to 500 μs less than the conditioner-probe interval in steps of 250 μs and for amplitudes of -30 dB, -24 dB, -12 dB and -6 dB relative to the resting threshold for a 10-μs pulse. (a) Sodium activation variable, *m*. (b) Sodium inactivation variable, *h*. (c) Potassium activation variable, *n*. (d) Non-specific ion channel activation variable, *p*.

Fig. 5. The relationships between the membrane potential, V, and (a) the steady-state value, h_∞, of the sodium inactivation variable, and (b) the time constant of the sodium inactivation variable, τ_h, in the FH model.

Fig. 6: Comparison between rate-level functions predicted from the modified LIF model and those calculated using the Frankenhaeuser-Huxley model. The parameters for the modified LIF model were optimized to get the best fit over all frequencies and are given in Table 1. The mean discharge rate (spikes/s) for the FH model at each stimulus level is shown by the solid dots and those for the modified LIF model are shown by the solid lines; the FH model is deterministic so no error bars are shown. The stimulus levels in each plot are in dB relative to threshold for the particular parameter set and stimulus frequency.

Fig. 7. Threshold recovery of the modified LIF model following an action potential, measured using a three-pulse paradigm for various amplitudes of a 1000-μs intermediate pulse. The threshold to the 10-μs probe pulse (the third pulse) against conditioner-probe interval (relative to the resting threshold) is shown for three levels of the intermediate pulse (solid circles: no intermediate pulse; open circles: -24 dB; solid triangles: -18 dB). The stimulus levels in dB are relative to the resting threshold of a 10-μs pulse. The solid lines shows the least-squares fit of a two time-constant refractory function (Equation 2).

Fig. 8. Optimum rate-level functions for the modified LIF model in response to sinusoidal stimulation from 50 Hz to 2 kHz (solid lines). The model parameters were optimized separately for each sciatic fibre, but for a given fibre the same parameters were used for all frequencies. The mean discharge rates for the sciatic nerve fibre are shown by the solid dots and the error bars show the standard deviation (5 presentations at each level); physiological data were not collected at all frequencies for all fibres. The stimulus levels are in dB relative to the threshold for the particular frequency.

Fig. 9. Comparison between the temporal response of the modified LIF model and sciatic nerve fibre X80LF3 showing (a) period histograms (PHs) and (b) inter-spike interval

histograms. Temporal response are shown for three frequencies (100 Hz, 500 Hz, and 1 kHz) and for stimulus levels from 1 to 9 dB above threshold. Results from X80LF3 are shown at the bottom of each plot and results from the modified LIF model are shown vertically offset. Because the conduction time of the fibre is unknown, the absolute phase between the stimulus and the response is unknown for the physiological experiments. An arbitrary horizontal offset has been added to the model PHs to aid comparison. The offset differs across frequency but for each frequency is constant across level.

Table 1

Parameter	FH model	Fibre X79LF6	Fibre X79RF1	Fibre X80LF3	Fibre X80LF5	Fibre X80RF1	Fibre X82RF3
τ (s)	1.39×10^{-3}	2.19×10^{-3}	2.34×10^{-3}	5.64×10^{-3}	1.83×10^{-3}	3.28×10^{-3}	4.28×10^{-3}
D	0	2.35×10^{-5}	3.59×10^{-6}	2.18×10^{-5}	1.52×10^{-5}	1.64×10^{-5}	5.00×10^{-5}
τ_{abs} (s)	7.80×10^{-5}	1.65×10^{-4}	3.06×10^{-5}	2.44×10^{-4}	1.50×10^{-3}	3.15×10^{-3}	1.48×10^{-3}
θ_M	2.644×10^{1}	1.94×10^{-1}	8.45×10^{-2}	3.57×10^{-1}	3.48×10^{-2}	1.31×10^{-1}	4.21×10^{-2}
μ_∞	6.44×10^{-1}	8.05×10^{-1}	8.41×10^{-1}	4.79×10^{-1}	1.36×10^{-2}	2.26×10^{-1}	1.30×10^{0}
σ_∞	1.26×10^{2}	1.94×10^{-2}	5.84×10^{-1}	1.16×10^{0}	1.03×10^{-1}	2.29×10^{-1}	1.43×10^{0}
τ_h (s)	1.36×10^{-3}	3.41×10^{-3}	2.23×10^{-2}	1.61×10^{-3}	1.52×10^{-3}	4.38×10^{-3}	1.54×10^{-2}
P	1.29	1.30	1.30	1.30	1.30	1.30	1.30

Figure 1 (2 columns)

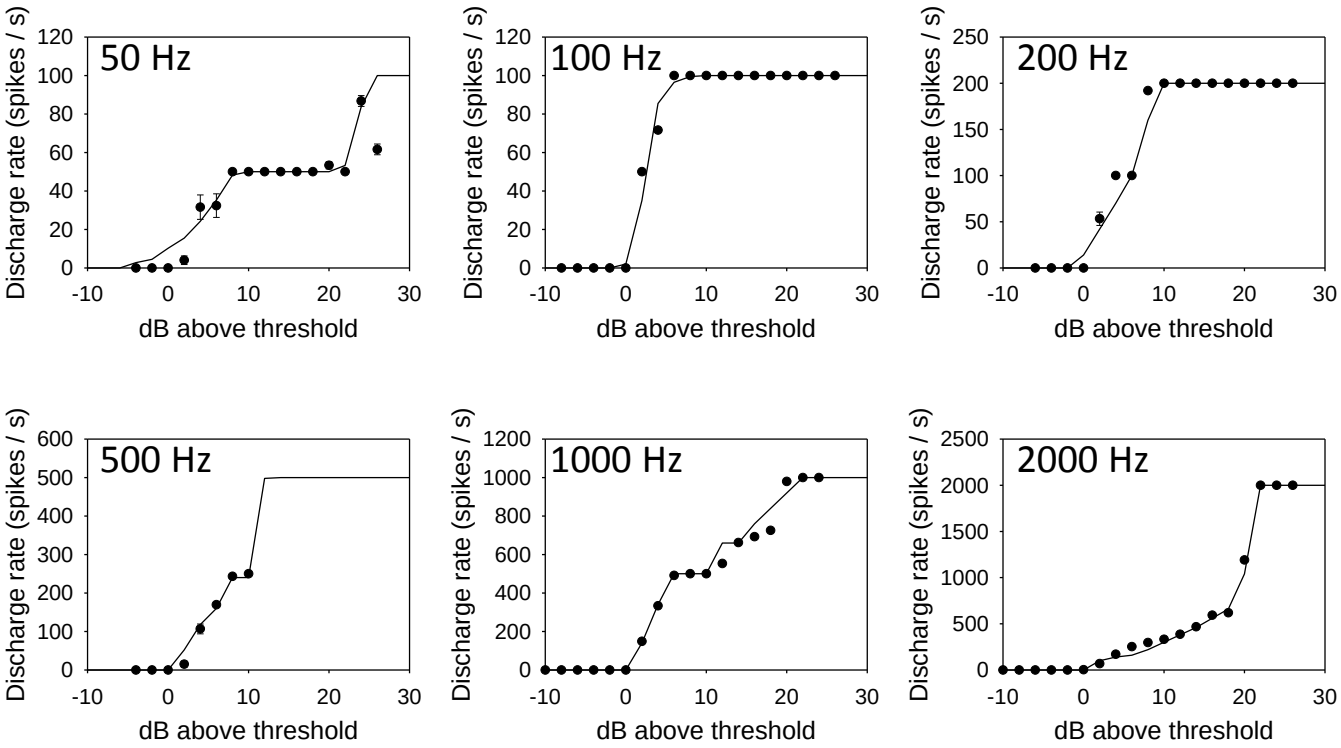

Figure 2 (1 column)

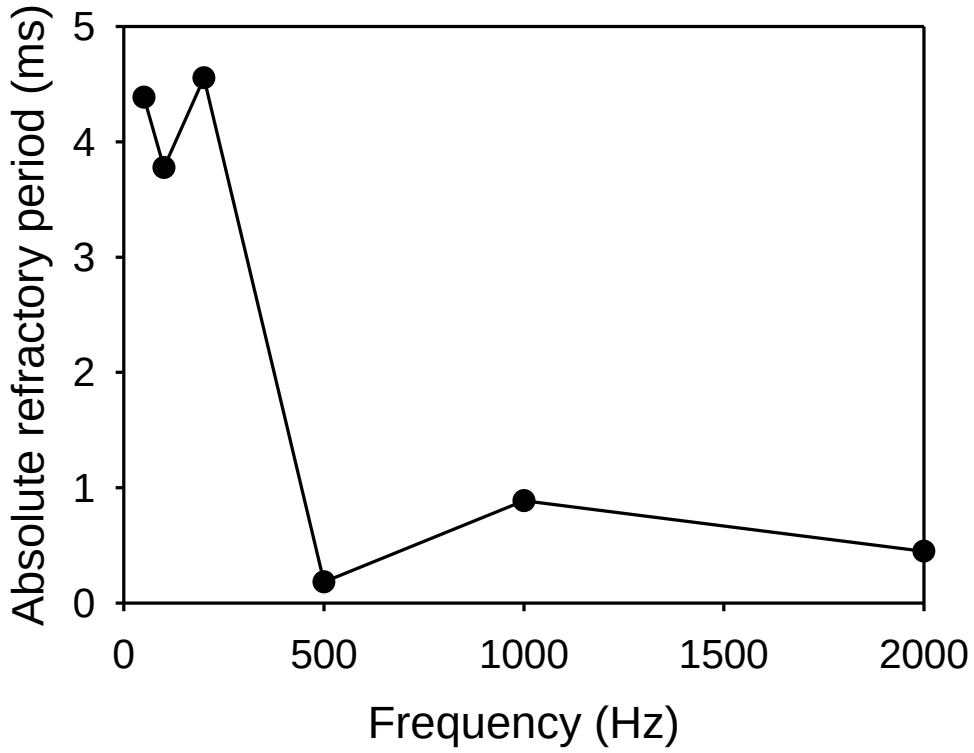

Figure 3 (2 columns)

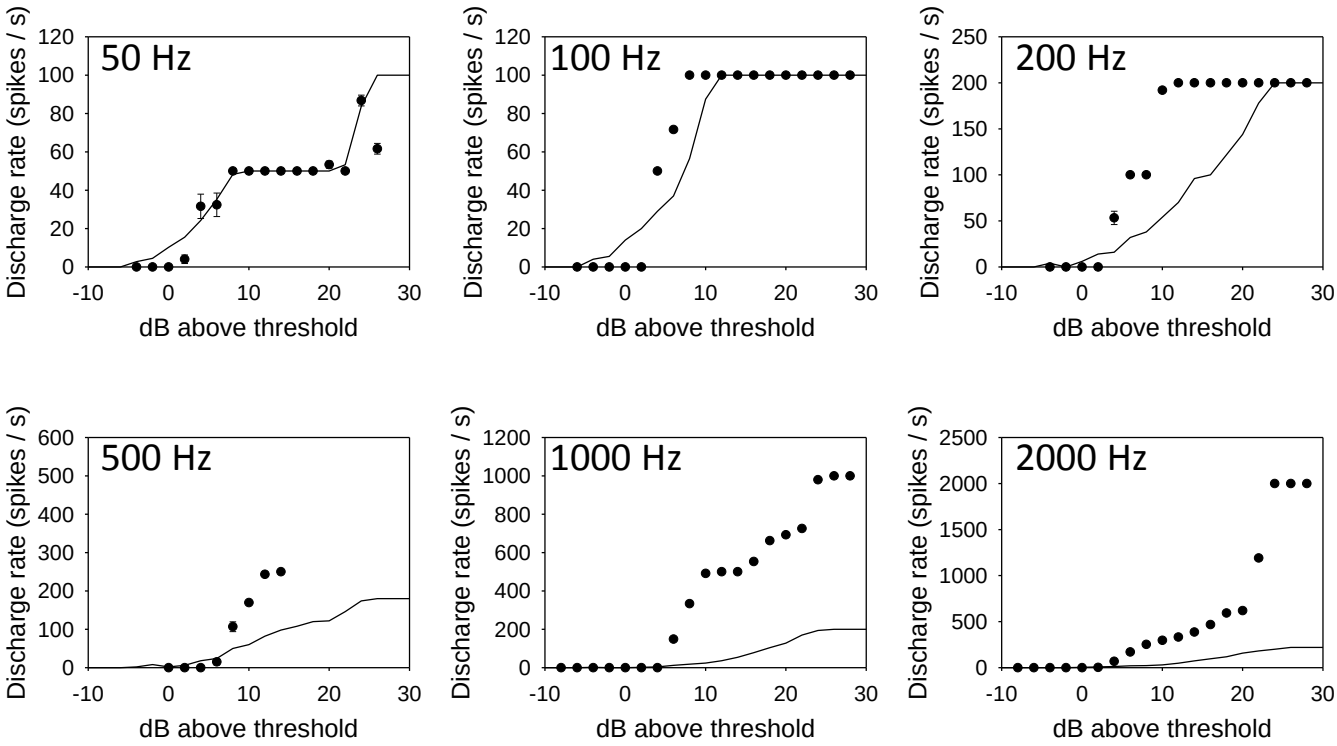

Figure 4 (2 columns)

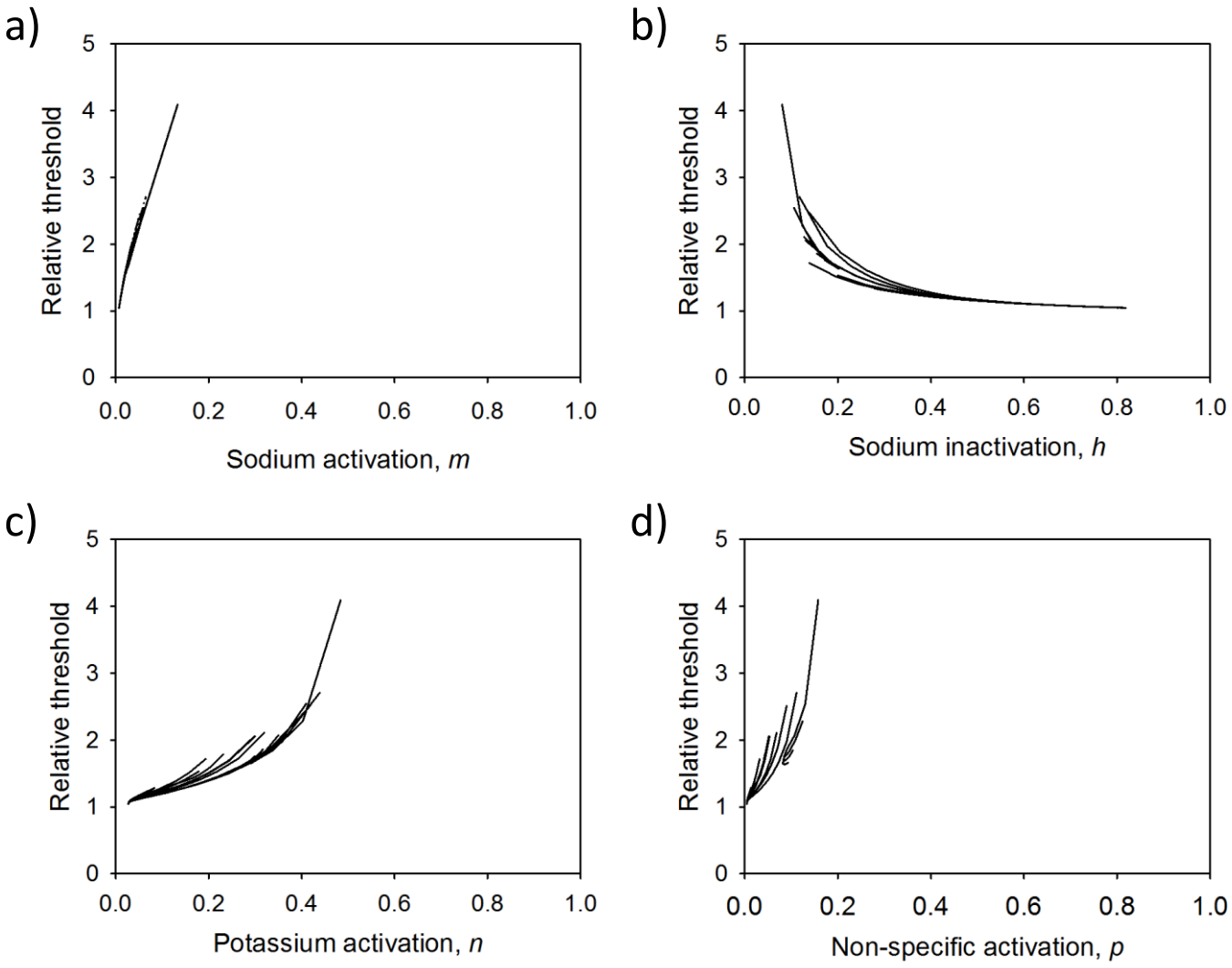

1 **Figure 5 (s columns)**

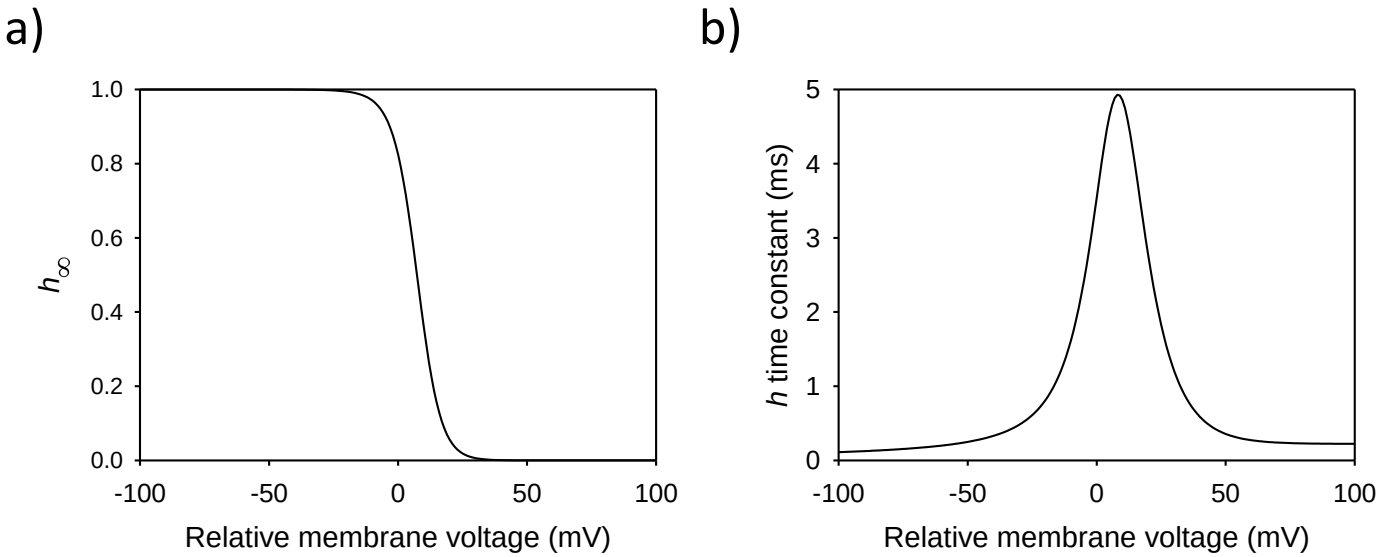

2

3 **Figure 6 (2 columns)**

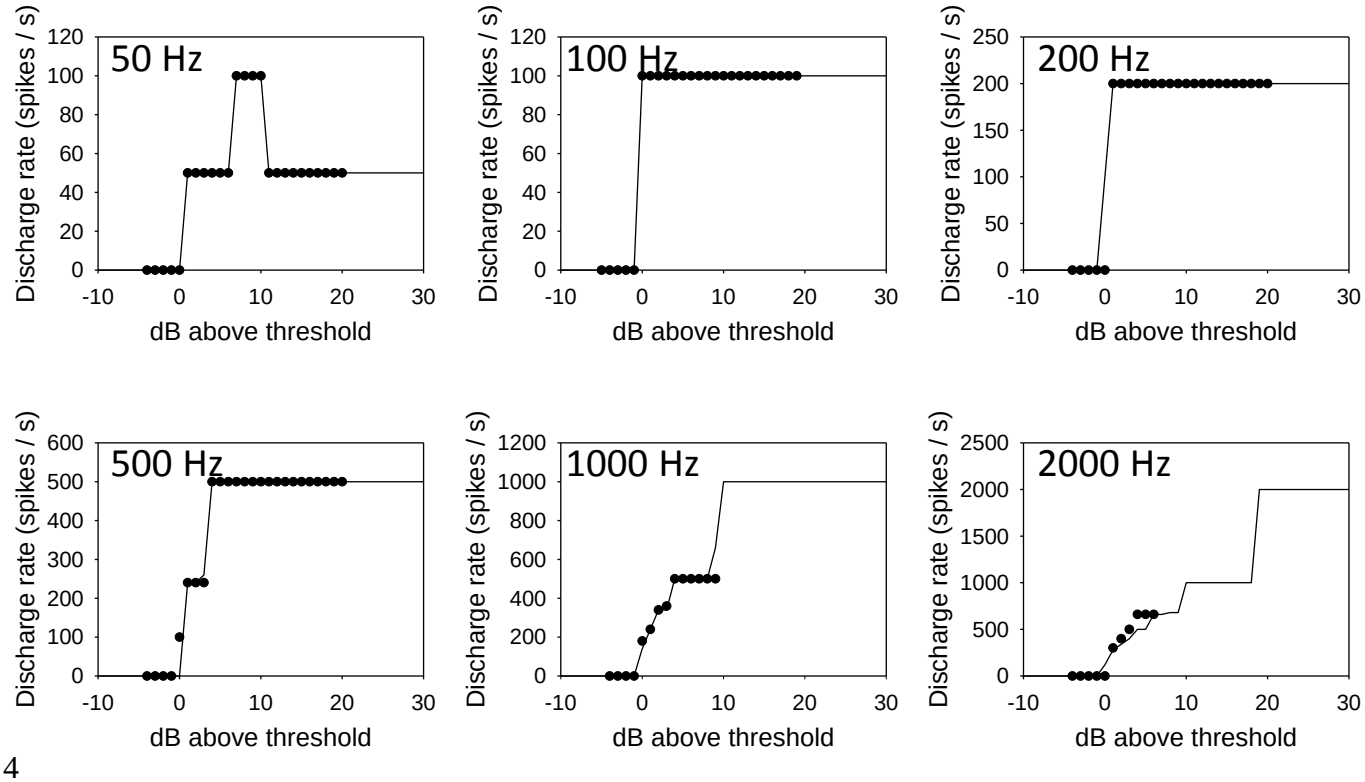

4

Figure 7 (1 column)

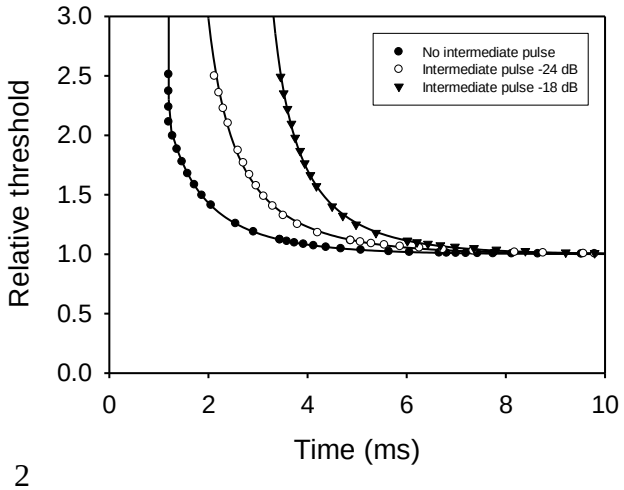

Figure 8 (2 columns)

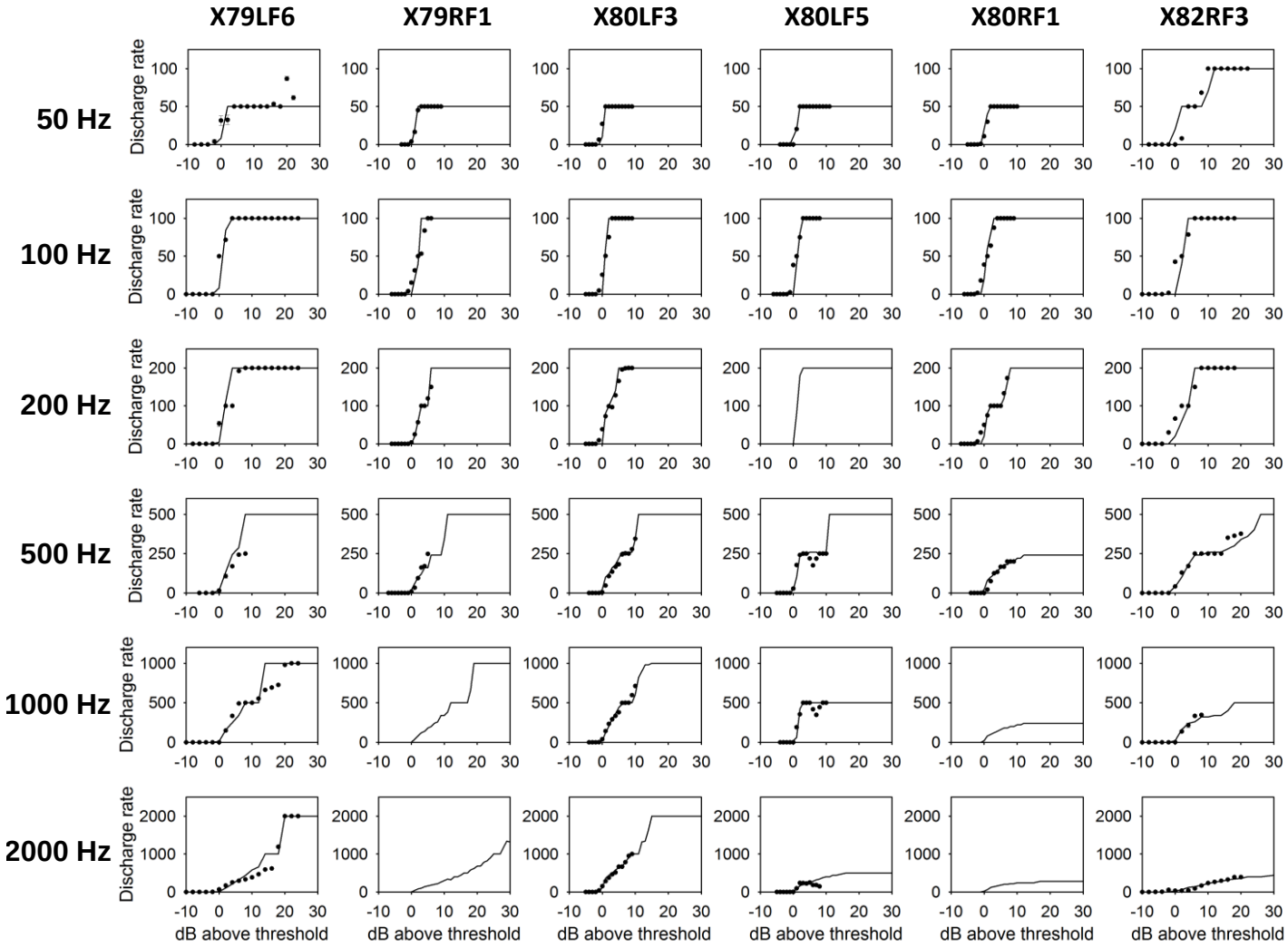

Figure 9 (2 columns)